Journal of Applied Physics

Defect annealing kinetics in ZnO implanted with Zn substituting elements: Zn interstitials and Li redistribution

Cite as: J. Appl. Phys. **125**, 075703 (2019); https://doi.org/10.1063/1.5083226
Submitted: 29 November 2018 . Accepted: 31 January 2019 . Published Online: 15 February 2019

Alexander Azarov, Bjørn L. Aarseth, Lasse Vines, Anders Hallén, Edouard Monakhov, and Andrej Kuznetsov

COLLECTIONS

EP This paper was selected as an Editor's Pick

ARTICLES YOU MAY BE INTERESTED IN

Bandgap of cubic $ZnS_{1-x}O_x$ from optical transmission spectroscopy
Journal of Applied Physics **125**, 075704 (2019); https://doi.org/10.1063/1.5064371

Luminescence of undoped commercial ZnS crystals: A critical review and new evidence on the role of impurities using photoluminescence and electrical transient spectroscopy
Journal of Applied Physics **125**, 075702 (2019); https://doi.org/10.1063/1.5084738

Electronic ground state analysis of Eu(II)-doped alkali-earth sulfide phosphors for photoluminescence properties
Journal of Applied Physics **125**, 075101 (2019); https://doi.org/10.1063/1.5059371

© 2019 Author(s).

Defect annealing kinetics in ZnO implanted with Zn substituting elements: Zn interstitials and Li redistribution

Cite as: J. Appl. Phys. **125**, 075703 (2019); doi: 10.1063/1.5083226
Submitted: 29 November 2018 · Accepted: 31 January 2019 ·
Published Online: 15 February 2019

Alexander Azarov,[1,2] Bjørn L. Aarseth,[1] Lasse Vines,[1] Anders Hallén,[3] Edouard Monakhov,[1] and Andrej Kuznetsov[1]

AFFILIATIONS

[1]Department of Physics, Centre for Material Science and Nanotechnology, University of Oslo, P.O. Box 1048, Blindern, N-0316 Oslo, Norway
[2]National Centre for Nuclear Research, A. Soltana 7, 05-400 Otwock-Swierk, Poland
[3]Royal Institute of Technology, KTH-ICT, Electrum 229, SE-164 40 Stockholm, Sweden

ABSTRACT

It is known that the behavior of residual Li in ion implanted ZnO depends on the preferential localization of the implants, in particular, forming characteristic Li depleted or Li pile-up regions for Zn or O sublattice occupation of the implants due to the corresponding excess generation of Zn and O interstitials in accordance with the so-called "+1 model." However, the present study reveals that conditions for the radiation damage annealing introduce additional complexity into the interpretation of the Li redistribution trends. Specifically, four implants residing predominantly in the Zn-sublattice, but exhibiting different lattice recovery routes, were considered. Analyzing Li redistribution trends in these samples, it is clearly shown that Li behavior depends on the defect annealing kinetics which is a strong function of the implanted fluence and ion species. Thus, Li depleted and Li pile-up regions (or even combinations of the two) were observed and correlated with the defect evolution in the samples. It is discussed how the observed Li redistribution trends can be used for better understanding a thermal evolution of point defects in ZnO and, in particular, energetics and migration properties of Zn interstitials.

Published under license by AIP Publishing. https://doi.org/10.1063/1.5083226

I. INTRODUCTION

ZnO is a direct wide bandgap semiconductor having numerous outstanding properties and potential applications in optoelectronics, spintronics, gas sensors, etc.[1,2] Non-toxicity, amenability to wet chemical etching, and availability of single crystalline material in addition to the large variety of nanostructure morphologies make ZnO an extremely promising material, which potentially can replace GaN—another wide bandgap semiconductor and currently a dominating material for optoelectronic devices operating in the blue and UV spectral range.[3] However, the doping asymmetry issue typical for II-VI semiconductors, where only n-type conductivity is easily achievable, limits the application prospects of ZnO.[4] The origin of this effect is still under debate, and one of the potential sources for the doping asymmetry is the native donor-type defects having low formation energy—zinc interstitials (Zn_i's) and oxygen vacancies (V_O), as well as their complexes.[4,5] The impact of these defects should be more pronounced in ion implanted ZnO because of radiation-induced defects. Furthermore, defects can mediate dopant diffusion,[6] affect magnetic properties,[7] and lead to the appearance of shallow acceptor states in ZnO, not directly related to the introduced dopant atoms.[8] Therefore, despite that ion implantation is a very attractive technological tool, which can be used for selective area doping at precise depth with a dopant concentration that can exceed the solubility, a better understanding of the formation and evolution of ion-induced defects is necessary.

Ion implantation-induced phenomena in ZnO have been intensively studied during the last decade.[9–29] In particular, it has been shown that ZnO exhibits extremely efficient dynamic annealing even at cryogenic temperatures, leading

Published under license by AIP Publishing.

to a high radiation tolerance.[9,10] Moreover, implantation parameters such as collision cascade density and an ion flux play a minor role in defect accumulation in ZnO.[11,27,28] However, defects of various types formed during ion bombardment[11–15] and post-implantation annealing are typically used to restore the crystalline structure and also to facilitate the substitution of the implanted ions at lattice sites.[16–24] The studies of ion-implanted ZnO have demonstrated highly intriguing features, where both the formation and annealing of ion-induced defects in ZnO strongly depend on the implanted species.[9,11,19,25,26] The specific dopant-defect reactions can lead to very unusual defect evolution upon annealing. For instance, it has been shown that defects induced by rare earth elements exhibit enhanced thermal stability as compared to other heavy ions, while damage in N implanted samples demonstrates anomalous reverse annealing where the damage increases during an early stage of the annealing.[19] These features considerably complicate the removal of ion-induced defects as well as the prediction of the final dopant distribution.

Meanwhile, it was shown that the behavior of residual group-Ia impurities, such as Li, can be efficiently used for investigating the preferential sublattice localization of implanted ions in ZnO.[29] In particular, it was concluded that Li depleted regions and Li pile-up regions form in the course of anneals of ZnO implanted with Zn and O-substituting elements, respectively. It was suggested that the formation of Li depleted regions is attributed to the interaction of Li atoms with Zn_i's injected from the damaged region. Indeed, in hydrothermally grown n-type ZnO, Li atoms preferentially occupy Zn sites (Li_{Zn}) and the formation of the Li depleted region is ascribed to fast moving interstitial Li (Li_i) formed via the kick-out reaction ($Zn_i + Li_{Zn} \rightarrow Zn_{Zn} + Li_i$).[29] An excess of Zn_i's needed for this reaction to occur is formed due to the preferential incorporation of implanted atoms on Zn sites, i.e., following the so-called "+1 model."[30] For clarity, this scenario is illustrated by the schematics in Fig. 1 where two possible mechanisms of Zn_i injection during the post-implant annealing are shown and labeled as (a) and (b). In particular, Fig. 1(a) corresponds to the case where the dopant atom wins a vacancy position over Zn_i, while Fig. 1(b) corresponds to the direct kick-out reaction of implanted species with the Zn atom situated in the lattice position. Both mechanisms should lead to the Zn_i excess in the implanted region. It should be noted that a third mechanism of Li depleted region formation could be considered for impurities which have a high diffusivity and can directly interact with Li. For example, it was demonstrated that Na starts to diffuse in ZnO already at the temperatures as low as 600 °C and the dominant trap for fast diffusing Na atoms is Li_{Zn}.[31] As a result, Na diffusion tail accompanied by a Li depleted region can form. However, this case is out of scope of the present work, where we study the evolution of ion-induced structural disorder concurrent with the redistribution of Li impurity in ZnO samples implanted with typical Zn-substituting elements, such as Er, Cd, and Si. We show that the kinetics of defect annealing plays a substantial role in Li redistribution and that the Li behavior can be used for the investigation of Zn/O type defect balance as well as defect evolution in ZnO during post-implant annealing.

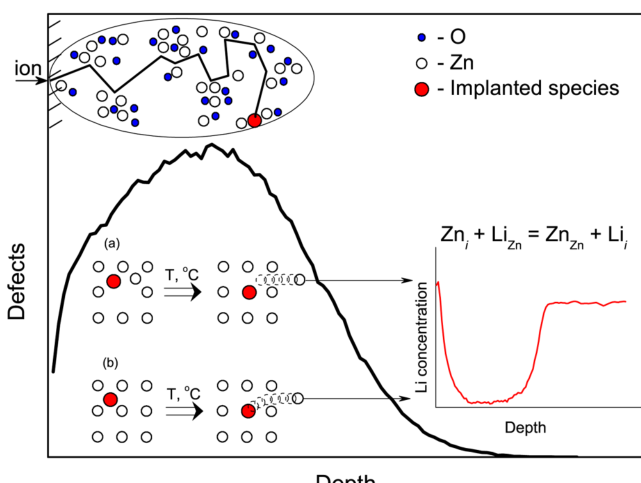

FIG. 1. Scenario of Zn_i's injection from the damaged region with subsequent kick-out reaction with substitutional Li in ZnO implanted with Zn substituting element (schematics of a single collision cascade and a typical depth profile of atomic displacements averaged over many cascades are shown for clarity). When annealed, the implanted species substitute for the Zn atom in its sublattice and two possible mechanisms of Zn_i injection, labeled (a) and (b), are shown. The inset also shows a Li depleted region formed due to a kick-out reaction of injected Zn_i with Li_{Zn} where Li atoms, transferred to the interstitial form, diffuse deeper into the bulk of the sample.

II. EXPERIMENTAL

Hydrothermally grown wurtzite (0001) ZnO single crystal wafers were implanted at room temperature with $^{166}Er^+$, $^{112}Cd^+$, and $^{28}Si^+$ ions to different fluences and energies, as indicated in Table I summarizing the implantation parameters used in the present study. Note that Er and Cd implants were carried out at 7° off the [0001] direction in order to reduce channeling, while Si implantation was deliberately performed along the [0001] direction. After implantation, the samples

TABLE I. Implantation parameters used in this study. The projected ranges (R_p) of implanted ions and the depth of maximum of the nuclear energy loss profiles (R_{pd}) were calculated with SRIM code[46] (notably, for Si, R_p was measured by SIMS as labeled with *). The Li residual content was found to be homogeneous through the as-implanted samples and also indicated in the table for reference.

Ion	Energy (keV)	Fluence (10^{15} cm^{-2})	R_p (nm)	R_{pd} (nm)	Tilt angle (deg)	Li (10^{17} cm^{-3})
^{166}Er	50	1.5	15	10	7	2
^{166}Er	200	0.8	40	27	7	2
^{112}Cd	250	5	60	40	7	2
^{28}Si	375	10	360/460*	260	0	0.2

Published under license by AIP Publishing.

were annealed in the temperature range of 500-1000 °C for 30 min in air. It should be noted that alternatively annealing can be performed in vacuum[32,33] or by electron beam irradiation.[34] However, vacuum annealing (including electron beam annealing, which typically requires high vacuum as well) can lead to a significant surface degradation.[33] Therefore, in order to avoid additional complications related to changing the defect balance at the surface and surface decomposition, all the anneals were performed in air, which was found to be sufficient in terms of avoiding surface alteration at the temperatures used in the present study.[33,35]

The ion-induced structural disorder was analyzed by Rutherford backscattering spectrometry in channeling mode (RBS/C) with 2.0 or 1.6 MeV $^4He^+$ ions backscattered into detectors placed at 100° and 165° relative to the incident beam direction. The so-called glancing-angle detector geometry (100°) was used to provide enhanced depth resolution specifically in the near-surface region, while the 165° backscattering angle was used to provide enhanced mass resolution to examine the behavior of the implanted ions. The RBS/C spectra were analyzed using a conventional algorithm,[36] allowing the determination of an effective number of interstitial defects (scattering centers). The fraction of implanted atoms occupying substitutional sites (non-scattering along the [0001] direction) was deduced by comparing the spectra obtained under channeling and random conditions, taking into account the shadowing effect. Therefore, the fraction of X atoms occupying Zn-sites has been calculated as $f_S^X = (1-\chi_{min}^X)/(1-\chi_{min}^{Zn})$, where χ_{min}^X and χ_{min}^{Zn} are integrated yields of the channeling spectra relative to the random ones in the region corresponding to the implanted area for X and Zn, respectively.

Li is one of the main residual impurities in the hydrothermally grown ZnO material, and the samples used in the present study contain Li with a concentration of 2×10^{17} cm^{-3} (for Er and Cd implants) or 2×10^{16} cm^{-3} (for Si implantation). Li concentration versus depth profiles were measured by secondary ion mass spectrometry (SIMS) using a Cameca IMS 7f microanalyzer with 10 keV O_2 ion as the primary beam for the analysis. The SIMS intensity to concentration calibration was performed using as-implanted samples as a reference, while the time to depth conversion was performed by measuring the crater depth using a Dektak 8 stylus profilometer and assuming a constant erosion rate.

III. RESULTS AND DISCUSSION

A. Role of the implanted fluence

Figure 2(a) shows RBS/C spectra of ZnO samples implanted with 50 keV Er ions to a fluence of 1.5×10^{15} cm^{-2} before and after annealing, and Fig. 2(b) shows the corresponding Li concentration versus depth profiles. The implantation leads to the formation of a pronounced defect peak positioned slightly deeper than the projected range, R_p. Figure 2(a) unveils that defect annealing starts near the surface already at 600 °C and then gradually proceeds from both sides of the disorder peak until nearly complete lattice recovery occurs at 1000 °C. Concurrently, the impact of the annealing on the substitutional fraction of Er atoms is illustrated by the inset in Fig. 2(a), plotting the non-scattering fraction of Er atoms as a function of annealing temperature. It is seen that almost all Er atoms are located at substitutional (non-scattering) positions already in the as-implanted state. However, Er atoms start to move out of their substitutional positions already at moderate temperatures (600 °C) and Er outdiffusion to the surface becomes pronounced at 800 °C. The 1000 °C anneal leads to a complete Er segregation at the surface.[37]

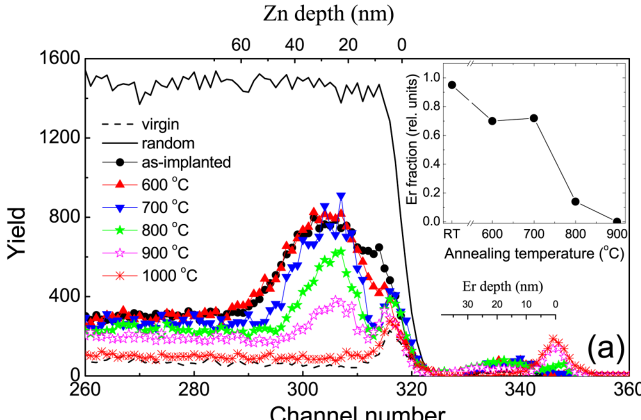

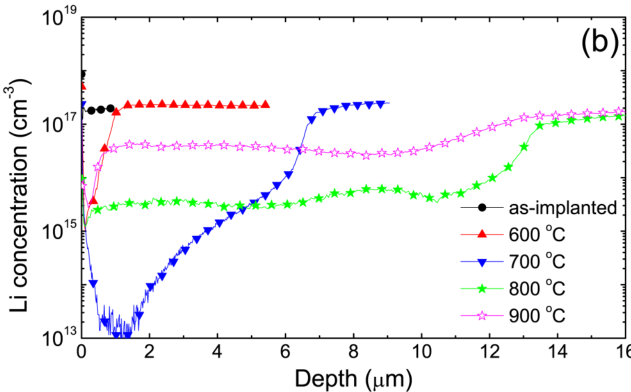

FIG. 2. (a) RBS/C spectra (acquired with 100° detector geometry and 2 MeV He^+ beam) of ZnO implanted with 50 keV Er ions to 1.5×10^{15} cm^{-2} before and after annealing as indicated in the legend and (b) corresponding Li concentration versus depth profiles as measured by SIMS. The substitutional (non-scattering) Er fraction as a function of annealing temperature is shown in the inset in panel (a).

It should be noted that the defect removal occurring at 600, 700, and 800 °C anneals is accompanied by a strong Li redistribution with the formation of a gradually advancing Li depleted region, extending up to 13 μm in depth after 800 °C [see Fig. 2(b)]. At higher temperatures, Li starts to diffuse back, refilling the depleted region (see the 900 °C Li profile). Such Li behavior was previously claimed to be typical for ZnO

Published under license by AIP Publishing.

implanted with Zn-substituting elements as discussed in Sec. I (Fig. 1). The only important difference of the process occurring in Fig. 2 from that shown in the schematics in Fig. 1 is that for Er most of the implanted atoms reside on Zn sides already in the as-implanted state, but this fraction decreases during the anneals [the inset in Fig. 2(a)]. Thus, both the kinetics of defect annealing and the evolution of the substitutional fraction of implanted atoms should be taken into account for the interpretation of Li redistribution at each specific annealing temperature.

For this purpose, Fig. 3 shows the amounts of Li atoms removed from the depleted region (ΔLi) and the number of displaced Zn atoms as a function of annealing temperature as deduced from SIMS and RBS/C data, respectively. It can be seen that a linear decrease of the amount of Zn sublattice defects in the temperature range of 600-900 °C is accompanied by a gradual increase of ΔLi. Further analysis can be performed normalizing ΔLi to the number of annealed defects (ΔLi_{def}) or to the fraction of the Er atoms located in substitutional positions (ΔLi_{Er}), and the values of ΔLi_{def} and ΔLi_{Er} as a function of annealing temperature are shown in the inset in Fig. 3. As mentioned in Sec. I, the mechanism of the formation of the Li depleted region involves the release of Zn_i's from the damaged region. Therefore, ΔLi_{def} and ΔLi_{Er} are dimensionless parameters indicating the efficiency of injection of Zn_i's relative to the defect annealing and Er incorporation, respectively.

According to the inset in Fig. 3, ΔLi_{Er} rapidly increases with temperature reaching ~1.3 after 800 °C. This result corroborates well with "+1 model"[30] where the total fluence of Er atoms incorporated in Zn sublattice equals to the number of Zn_i's injected into the bulk and reacted with Li atoms. It should be noted that the formation of stable vacancy related complexes can affect an excess of Zn_i's, so the magnitude of ΔLi_{Er} in excess of unity may indicate a stabilization of V_{Zn} via the formation of Er-related defect complexes. At lower temperatures (600 and 700 °C), ΔLi_{Er} is far below unity indicating that there is another factor limiting the number of Zn_i's released from the damaged region. In fact, the balance between the processes of defect annihilation and release of Zn_i's determines ΔLi_{def}, and the inset in Fig. 3 shows that ΔLi_{def} does not exceed 1%. Such a low value of ΔLi_{def} indicates that the efficiency of Zn_i injection into the crystal bulk is relatively low, and the major part of defects annihilate within the damaged region.

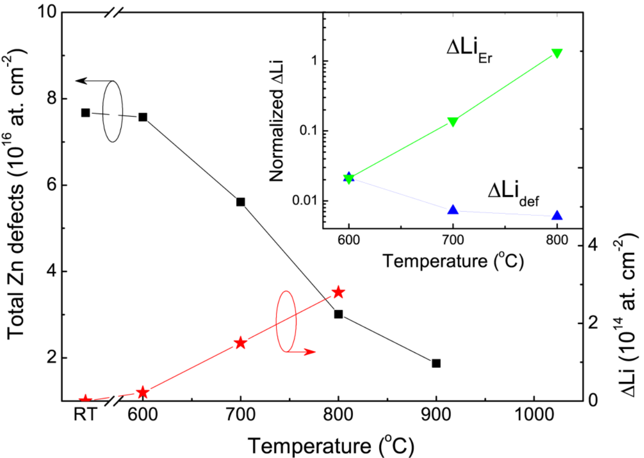

FIG. 3. Amount of Li removed from the depletion region (ΔLi) as deduced from SIMS data (stars, right-hand scale) and total number of displaced Zn atoms (scattering centers) as deduced from RBS/C data (squares, left-hand scale) as a function of annealing temperature. The inset shows the ΔLi normalized to the substitutional Er fraction (ΔLi_{Er}) and to the number of defects annealed (ΔLi_{def}) as a function of temperature.

It should be noted that exact mechanism of Zn_i injection for Er implants is not well understood and it could be different from that for other ion species. For example, it was demonstrated that Zn precipitation formation and Li depletion are well correlated in Zn implanted ZnO single crystals.[38] Specifically for Er, a formation/dissociation of optically active defect centers in the course of annealing can play a role.[21] Furthermore, a large strain can be accumulated in heavily damaged crystals and it was shown that this strain may act as a driving force for defect transformation with increasing ion fluence.[15] Evidently, release of the strain due to defect thermal evolution may also affect Zn_i behavior. However, more work is needed to reveal and generalize the mechanisms of Zn_i injection from the damaged area into the bulk.

The defects in the samples implanted with about half the Er fluence used in Fig. 2 and higher energy exhibit a very different behavior with temperature as compared to the high fluence case shown in Fig. 2. Indeed, the disorder profiles in the samples implanted with 200 keV Er ions to 8×10^{14} cm^{-2} [Fig. 4(a)] exhibit an intriguing multipeak defect distribution with a well-defined intermediate peak (shown by the arrow and labeled as IP) in between the conventionally expected surface and bulk damage peaks labeled as SP and BP, respectively. Annealing at ≤800 °C does not affect the defect distribution but results in some "sharpening" of the IP. Heat treatment at 900 °C leads to removal of the IP and further increase of the annealing temperature results in almost complete lattice recovery as well as Er outdiffusion, resembling the behavior of the high fluence sample [Fig. 2(a)].

Importantly, irrespective of the implanted fluence, the substitutional Er fraction shows a similar trend as a function of temperature [insets in Figs. 2(a) and 4(b)]. However, the corresponding Li behavior is different, as seen from the comparison of Figs. 2(b) and 4(b). Indeed, already upon the 700 °C anneal, Li pile-up is observed at the depth around R_{pd} [shown by the dashed line in Fig. 4(b)] and a relatively weak Li depleted region forms right behind the R_{pd}. After 800 °C, the Li pile-up around R_{pd} becomes more pronounced, while the Li depleted region practically vanishes. The absence of the Li depletion is consistent with minor defect annealing at the temperatures up to 800 °C and, therefore, negligible Zn_i injection as may be expected from the RBS/C results [Fig. 4(a)]. At this end, it may be concluded that the mechanism labeled

Published under license by AIP Publishing.

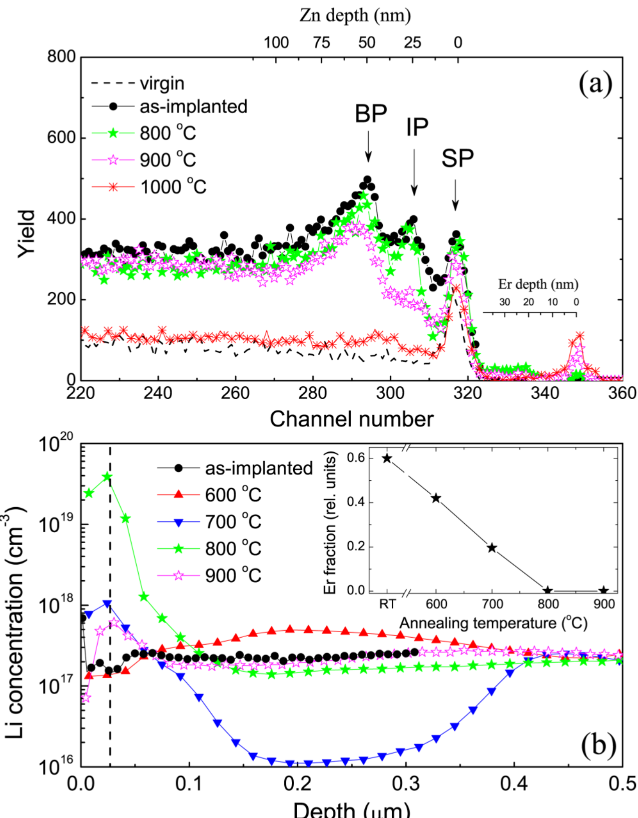

FIG. 4. RBS/C spectra (acquired with 100° detector geometry and 2 MeV He$^+$ beam) of ZnO implanted with 200 keV Er ions to 8×10^{14} cm^{-2} before and after annealing as indicated in the legend [the random spectrum is similar to that shown in Fig. 2(a)]. Corresponding Li concentration versus depth profiles as measured by SIMS are shown in panel (b). The vertical, dashed lines in panel (b) mark the R_{pd} of the implanted ions. The substitutional (non-scattering) Er fraction as a function of annealing temperature is shown in the inset in panel (b).

as (a) in Fig. 1 plays a dominant role on Zn_i injection from the damaged region for Er.

It should be noted that the Li pile-up around R_{pd} is quite intriguing. Indeed, previously, Li accumulation at the depth of the implanted damage peak was observed in ZnO implanted with O[39] and O-substituting elements such as N.[29] The observation was attributed to the Li trapping via the formation of Li_{Zn}-O_i complexes that are likely to occur under O-rich conditions.[40] Evidently, an excess of O_i's is needed for the efficient formation of such complexes and the surplus of O_i was thought to occur because of the preferential incorporation of the implanted species on the O-sites. However, in Fig. 4 we do not observe this correlation as the major part of implanted Er atoms occupies non-substitutional sites after 800 °C anneals [see the inset in Fig. 4(b)], and therefore, other processes should be responsible for the accumulation of Li. One process could be an enhanced vacancy clustering in the damaged region, and therefore, the Li pile-up can be attributed to efficient Li trapping at open-volume defects.[41] Surprisingly, our results reveal the potential role of IP defects in Li trapping. Indeed, the position of the Li pile-up corresponds well to the IP in the defect distribution [Figs. 4(a) and 4(b)], and the Li pile-up dramatically decreases at the temperature when the IP becomes unstable (900 °C). Although the formation of an IP was previously observed in ZnO samples implanted by ions generating dense collision cascades, the mechanisms of the IP formation are not well understood.[11,13,20,27] Myers *et al.*[13] have suggested that the IP is related to an interface between Zn-rich extended defects and near the surface nano-cavities, which can explain Li trapping at this range too. The formation of an O deficient region between the sample surface and R_p implanted ions was also recently reported for Yb implanted ZnO single crystals by high resolution SIMS measurements.[42] One of the possible reasons for the formation of open volume defects can be related to local stoichiometric disturbances in the collision cascades.[43] Therefore, an enhanced concentration of O vacancies is expected in the near surface region and this process can affect both Li and dopant redistribution after annealing, as demonstrated recently in Ref. 44. It is important to note that our results also indicate a different nature of the defects in the IP as compared to either SP or BP.

B. Two stage damage annealing

Cd is an almost ideal Zn-substituting element in ZnO,[45] and in contrast to Er, the substitutional Cd fraction increases with temperature and reaches ~95% after 800 °C anneals [see the inset in Fig. 5(a)]. Figure 5(a) shows the RBS/C spectra of the samples implanted with Cd before and after different anneals. It can be seen that the implantation produces a strong damage peak around R_p, and the defect annealing for Cd seems to proceed in two stages. The first stage occurs at ≤500 °C and is associated with a strong annealing of uncorrelated defect structures, such as point defects and small defect clusters, mainly situated around R_p. It can also be noted that the substitutional fraction of Cd decreases from about 90% in the as-implanted case (similar to higher fluence Er) to about 40% after 500 °C and then returns to a nearly full substitutional fraction upon further annealing. The high dechanneling yield without a well defined damage peak after annealing, as seen in Fig. 5(a) at depths larger than R_p, indicates predominantly extended defects and the second stage is attributed to gradual annealing of these defects at higher temperatures as clearly seen from the decreasing RBS/C yield. It has also been suggested that extended defects act as strong sinks for mobile point defects and, therefore, play a substantial role in the defect evolution at the first stage.[14]

However, in spite of the high substitutional Cd fraction, the Li depletion is rather modest reaching ~3 μm only after 800 °C as illustrated by Fig. 5(b), showing the Li concentration vs depth profiles in the Cd implanted samples after 600 and 800 °C anneals. The integrated amount of removed Li

Published under license by AIP Publishing.

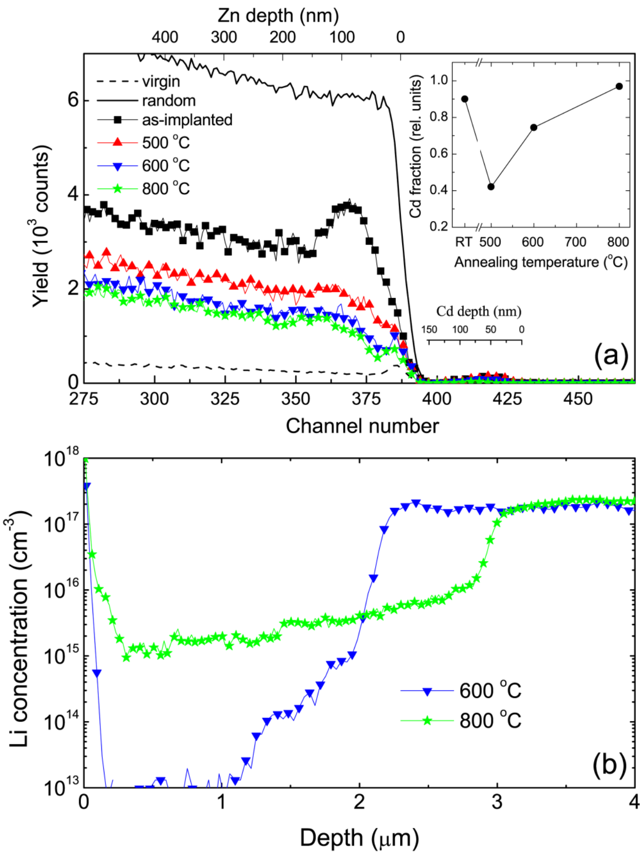

FIG. 5. (a) RBS/C spectra (acquired with 165° detector geometry and 2 MeV He^+ beam) of ZnO implanted with 250 keV Cd ions to $5 \times 10^{15}\,cm^{-2}$ before and after annealing as indicated in the legend and (b) corresponding Li concentration versus depth profiles as measured by SIMS. The substitutional (non-scattering) Cd fraction as a function of annealing temperature is shown in the inset in panel (a).

normalized to the amount of substitutional Cd atoms, ΔLi_{Cd}, is about 0.012 for both annealing temperatures. Such a low value of ΔLi_{Cd} indicates that injection of Zn_i's from the damaged region at the second annealing stage is limited. Furthermore, in strong contrast to Er, Zn_i injection due to the direct kick out reaction [see the mechanism Fig. 1(b)] cannot be excluded.

C. Thermal stability of extended defects

Previously, it has been shown that the sample orientation in relation to the incident beam primarily affects the amount of uncorrelated defect structures, while the formation of extended defects, such as stacking faults or dislocation loops, has a weak dependence on ZnO crystal orientation.[14] Therefore, the samples were implanted by Si ions along the [0001] direction in order to create predominantly extended defects. Figure 6 shows RBS/C spectra of the Si implanted

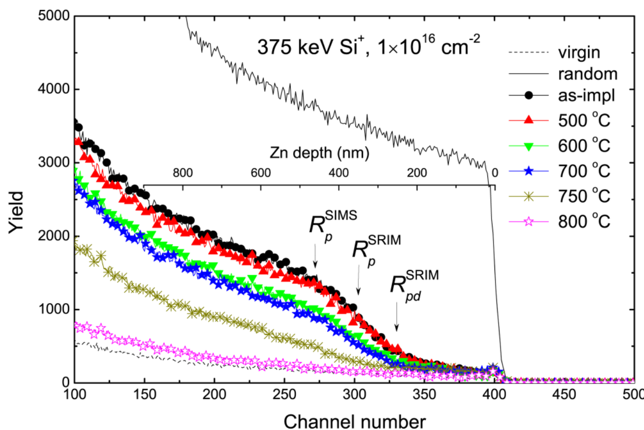

FIG. 6. RBS/C spectra (acquired with 165° detector geometry and 1.6 MeV He^+ beam) of ZnO implanted along the [0001] direction with 375 keV Si ions to $1 \times 10^{16}\,cm^{-2}$ before and after annealing, as indicated in the legend. SRIM-predicted[46] R_p and R_{pd} as well as R_p measured by SIMS of the implanted ions in correlation with the Zn depth scale are shown by the arrows.

samples, and the spectrum of the as-implanted sample demonstrates a shape with high dechanneling behind R_{pd} without a well-defined damage peak. Such spectrum shape is typical for the samples where extended defects dominate[14,15] and corroborate with previously reported results on channeling implantations into ZnO single crystals.[14] It is worth to notice that defect annealing kinetics in the samples implanted with Si exhibits quite intriguing behavior different from other cases. Indeed, Fig. 6 shows that Si induced defects are stable at the temperatures up to 500 °C, while 600 °C annealing leads to the rapid recovery of the crystalline structure and RBS/C spectrum of the 800 °C annealed sample almost resembles the unimplanted one, indicating practically complete defect annealing.

It should be noted that, in contrast to point defects and small defect clusters, a complete removal of ion-induced extended defects in ZnO typically requires relatively high temperatures exceeding 900-1000 °C as reported for other ion species including Ag (Ref. 14), Au (Ref. 19), and N (Ref. 47). Furthermore, the implanted atoms themselves can stabilize radiation defects while pronounced loss or out-diffusion of implanted atoms may lead to an efficient recovery of the crystalline lattice.[19] However, this is not the case for Si implanted samples since our measurements reveal only a minor Si redistribution for the temperatures up to 800 °C (not shown) and other mechanisms involving implanted Si atoms should be considered. Despite that Si is a promising donor impurity in ZnO that could be used for a fabrication of transparent conductive oxides,[48] there are only a few reports on defect behavior in Si implanted ZnO.[11,49,50] Importantly, it was demonstrated that, in contrast to many other ion species, dopant-defect reactions dominate the damage formation for Si implanted ZnO, which can even lead to amorphization of ZnO.[11] Exact mechanisms of the enhanced defect formation

Published under license by AIP Publishing.

for Si implantation are not well understood, but it has been suggested that the formation of SiO_x inclusions can play a role.[49] It was suggested that increasing the concentration of open volume defects during post-implant annealing in Si implanted samples can be associated with the formation and growth of such inclusions.[49] Using positron annihilation, it was furthermore demonstrated that the concentration of open volume defects reaches its maximum at 700 °C and annealing at higher temperatures leads to the removal of these defects. It can be speculated that high concentration of open volume defects affects the thermal evolution of extended defects, leading to efficient recovery of the crystal lattice already at moderate temperatures.

Additional information about defect annealing kinetics can be obtained from Li behavior, and the Li concentration versus depth profiles for the Si-implanted samples are shown in Fig. 7. The position of R_p, as measured by SIMS, is depicted by the dashed line. Surprisingly, Li atoms exhibit a behavior typical for both Zn and O-substituting elements. Indeed, Li atoms exhibit a minor redistribution for temperatures up to 600 °C; however, 700 °C anneal leads to the formation of a pronounced Li depletion extending up to ~17 μm beyond R_p and some Li accumulation in the region close to R_{pd}/R_p. Annealing at higher temperatures results in further growth of the Li depletion so that it extends up to ~100 μm after 800 °C anneal. In addition, the Li atoms form even more prominent pile-up around R_{pd}/R_p with a peak concentration at 5×10^{18} cm^{-3}, exhibiting a shoulder extending up to 15 μm into the bulk of the sample. In contrast to Er and Cd implants, the substitutional fraction of Si atoms is not possible to estimate using RBS/C results alone, because of the relatively low Si mass. However, formation of a Li depleted region indicates at least partial incorporation of Si atoms on Zn sublattice.

It should be noted that, an extremely wide Li depletion for Si may indicate also that Li_{Zn} is a dominant trap for fast diffusing Zn_i's. Previously, it was demonstrated that substantial injection of Zn_i's occurs relatively fast and a saturation of Li depletion was observed already after ~30 s anneals.[39] Therefore, in order to estimate an effective diffusivity of Zn_i's (D_{Zn}), we use a characteristic time equal to 30 s and Fig. 8 shows Arrhenius plots of the D_{Zn} calculated as a square of the width of the Li depleted region divided by this characteristic time scale. This simple approach shown in Fig. 8 revealed activation energies (E_a) of the effective Zn_i diffusion (D_{Zn}) of 3.1 and 2.1 eV for Si and 50 keV for Er implants, respectively. Note that the obtained values of E_a are higher than that obtained from electrical measurements of low fluence He-implanted samples, where authors reported that E_a of Zn interstitials is 0.75 eV.[52] However, this difference is not surprising because of the different nature of the damage formed under low and high fluence implantation regimes, as well as different ion species used. In its turn, a difference in absolute values of D_{Zn} for different implants can be attributed to the different quality of the samples used for Er and Si implantations and, therefore, different concentration of trapping centers in these samples.

Finally, note that pile-up of Li around R_p does not necessary indicate that Si atoms readily substitute O-sites (Si_O) in this region. Instead, as mentioned above, formation of SiO_x inclusions is possible in Si implanted samples. These inclusions can lead to the stabilization of oxygen vacancies, which are efficient traps for Li atoms. Moreover, Si_{Zn} acts as a donor, so incorporation of Si atoms on the Zn sublattice should lift the Fermi level position in the implanted region. In its turn, the formation energy of V_{Zn} decreases as the Fermi level moves toward the conduction band,[6,51] and therefore, the probability of trapping of Li atoms by V_{Zn}'s increases.

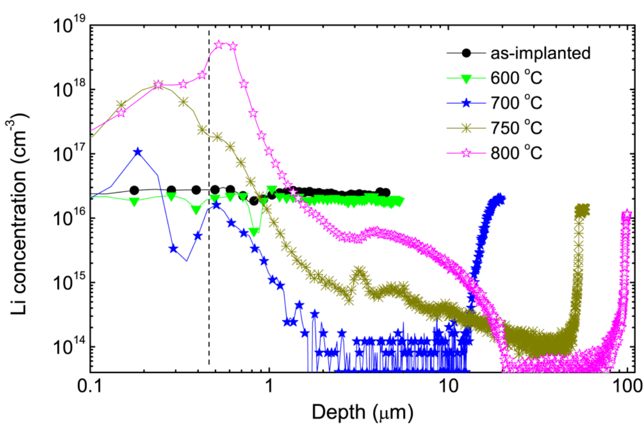

FIG. 7. (a) Li concentration versus depth profiles as measured by SIMS in the Si implanted samples before and after annealing, as indicated in the legends. R_p of the implanted ions as measured by SIMS is shown by the vertical dashed line.

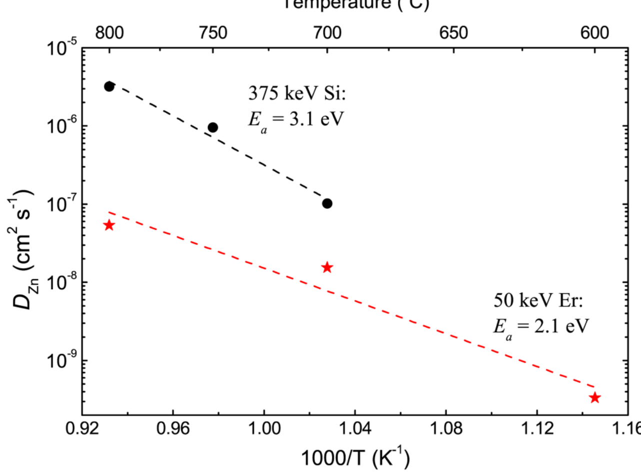

FIG. 8. Arrhenius plots of the effective Zn_i diffusion as a function of reciprocal temperature for 50 keV Er (stars) and 375 keV Si (circles) implants (see the text for details).

Published under license by AIP Publishing.

IV. CONCLUSIONS

The interaction of point defects and defect complexes with residual impurities, such as Li, provides a possibility to better understand the kinetics of defect annealing in ion implanted ZnO, which depends also on ion species and implanted fluence. For Er, the heavily damaged samples exhibit a single stage annealing behavior with gradual recovery of crystal lattice accompanied by the formation of the pronounced Li depleted region, indicating efficient injection of Zn_i's from the implanted region into the bulk. In contrast, for lower Er fluence, the implantation damage occurs in the form of a multipeak distribution. This defect structure is found to be quite stable at temperatures ≤800 °C and Li pile-up in the vicinity of the implanted region meaning no, or very limited Zn_i injection into the bulk of ZnO. High fluence Cd implanted samples exhibit a two stage defect annealing behavior, where the second stage at >500 °C is associated with gradual recovery of extended defects. This stage is likely to be accompanied with a low rate Zn_i injection leading to the formation of relatively limited Li depletion in spite of a high Cd substitutional fraction. In its turn, the extended defects produced by channeled Si implantation show lower thermal stability as compared to those for Cd and almost complete crystal recovery occurs already after 800 °C. Annealing of Si-induced defects is also accompanied by Li redistribution typical for both O- and Zn-substituting elements, which indicates the formation of open volume defects around the R_{pd}/R_p region and simultaneous injection of Zn_i's into the bulk during the anneals.

ACKNOWLEDGMENTS

Financial support was kindly provided by the Research Council of Norway and University of Oslo through the frontier research project FUNDAMeNT (Project No. 251131, FriPro ToppForsk-program). The Research Council of Norway is also acknowledged for the support to the Norwegian Micro- and Nano-Fabrication Facility, NorFab (Project No. 245963).

REFERENCES

[1]Ü. Özgür, Y. I. Alivov, C. Liu, A. Teke, M. A. Reshchikov, S. Doğan, V. Avrutin, S.-J. Cho, and H. Morkoç, "A comprehensive review of ZnO materials and devices," J. Appl. Phys. **98**, 041301 (2005).

[2]A. B. Djurišić, A. M. C. Ng, and X. Y. Chen, "ZnO nanostructures for optoelectronics: Material properties and device applications," Prog. Quant. Electron. **34**, 191 (2010).

[3]S. J. Pearton, J. C. Zolper, R. J. Shul, and F. Ren, "GaN processing, defects, and devices," J. Appl. Phys. **86**, 1 (1999).

[4]C. H. Park, S. B. Zhang, and S.-H. Wei, "Origin of *p*-type doping difficulty in ZnO: The impurity perspective," Phys. Rev. B **66**, 073202 (2002).

[5]S. B. Zhang, "The microscopic origin of the doping limits in semiconductors and wide-gap materials and recent developments in overcoming these limits: A review," J. Phys. Condens. Matter **14**, R881 (2002).

[6]A. Azarov, V. Venkatachalapathy, Z. Mei, L. Liu, X. Du, A. Galeckas, E. Monakhov, B. G. Svensson, and A. Kuznetsov, "Self-diffusion measurements in isotopic heterostructures of undoped and in situ doped ZnO: Zinc vacancy energetics," Phys. Rev. B **94**, 195208 (2016).

[7]Q. Xu, H. Schmidt, S. Zhou, K. Potzger, M. Helm, H. Hochmuth, M. Lorenz, A. Setzer, P. Esquinazi, C. Meinecke, and M. Grundmann, "Room temperature ferromagnetism in ZnO films due to defects," Appl. Phys. Lett. **92**, 082508 (2008).

[8]M. Schirra, R. Schneider, A. Reiser, G. M. Prinz, M. Feneberg, J. Biskupek, U. Kaiser, C. E. Krill, K. Thonke, and R. Sauer, "Stacking fault related 3.31-eV luminescence at 130-meV acceptors in zinc oxide," Phys. Rev. B **77**, 125215 (2008).

[9]A. Y. Azarov, E. Wendler, A. Y. Kuznetsov, and B. G. Svensson, "Crucial role of implanted atoms on dynamic defect annealing in ZnO," Appl. Phys. Lett. **104**, 052101 (2014).

[10]K. Lorenz, E. Alves, E. Wendler, O. Bilani, W. Wesch, and M. Hayes, "Damage formation and annealing at low temperatures in ion implanted ZnO," Appl. Phys. Lett. **87**, 191904 (2005).

[11]S. O. Kucheyev, J. S. Williams, C. Jagadish, J. Zou, C. Evans, A. J. Nelson, and A. V. Hamza, "Ion-beam-produced structural defects in ZnO," Phys. Rev. B **67**, 094115 (2003).

[12]G. Perillat-Merceroz, P. Gergaud, P. Marotel, S. Brochen, P.-H. Jouneau, and G. Feuillet, "Formation and annealing of dislocation loops induced by nitrogen implantation of ZnO," J. Appl. Phys. **109**, 023513 (2011).

[13]M. T. Myers, S. Charnvanichborikarn, C. C. Wei, Z. P. Luo, A. Aitkaliyeva, L. Shao, and S. O. Kucheyev, "Defect microstructure in heavy-ion-bombarded (0001) ZnO," Acta Mater. **60**, 6086 (2012).

[14]A. Azarov, P. Rauwel, A. Hallén, E. Monakhov, and B. G. Svensson, "Extended defects in ZnO: Efficient sinks for point defects," Appl. Phys. Lett. **110**, 022103 (2017).

[15]A. Turos, P. Jóźwik, M. Wójcik, J. Gaca, R. Ratajczak, and A. Stonert, "Mechanism of damage buildup in ion bombarded ZnO," Acta Mater. **134**, 249 (2017).

[16]E. Rita, E. Alves, U. Wahl, J. G. Correia, T. Monteiro, M. J. Soares, A. Neves, and M. Peres, "Stability and luminescence studies of Tm and Er implanted ZnO single crystals," Nucl. Instrum. Methods B **242**, 580 (2006).

[17]A. Y. Azarov, A. Hallén, B. G. Svensson, and A. Y. Kuznetsov, "Annealing of ion implanted CdZnO," J. Phys. D **45**, 235304 (2012).

[18]S. M. C. Miranda, M. Peres, T. Monteiro, E. Alves, H. D. Sun, T. Geruschke, R. Vianden, and K. Lorenz, "Rapid thermal annealing of rare earth implanted ZnO epitaxial layers," Opt. Mater. **33**, 1139 (2011).

[19]A. Y. Azarov, A. Hallén, P. Rauwel, X. L. Du, A. Y. Kuznetsov, and B. G. Svensson, "Effect of implanted species on thermal evolution of ion-induced defects in ZnO," J. Appl. Phys. **115**, 073512 (2014).

[20]L. M. C. Pereira, J. P. Araújo, U. Wahl, S. Decoster, M. J. Van Bael, K. Temst, and A. Vantomme, "Searching for room temperature ferromagnetism in transition metal implanted ZnO and GaN," J. Appl. Phys. **113**, 023903 (2013).

[21]A. Azarov, A. Galeckas, A. Hallén, A. Kuznetsov, E. Monakhov, and B. G. Svensson, "Optical activity and defect/dopant evolution in ZnO implanted with Er," J. Appl. Phys. **118**, 125703 (2015).

[22]A. Audren, A. Hallén, M. K. Linnarsson, and G. Possnert, "Damage recovery in ZnO by post-implantation annealing," Nucl. Instrum. Methods B **268**, 1842 (2010).

[23]R. Ratajczak, S. Prucnal, E. Guziewicz, C. Mieszczynski, D. Snigurenko, M. Stachowicz, W. Skorupa, and A. Turos, "The photoluminescence response to structural changes of Yb implanted ZnO crystals subjected to non-equilibrium processing," J. Appl. Phys. **121**, 075101 (2017).

[24]A. Turos, R. Ratajczak, C. Mieszczynski, P. Jozwik, A. Stonert, S. Prucnal, R. Heller, W. Skorupa, J. von Borany, and E. Guziewicz, "Ion beam modification of ZnO epilayers: Sequential processing," Phys. Status Solidi A **215**, 1700887 (2018).

[25]Z. Q. Chen, M. Maekawa, A. Kawasuso, S. Sakai, and H. Naramoto, "Annealing process of ion-implantation-induced defects in ZnO: Chemical effect of the ion species," J. Appl. Phys. **99**, 093507 (2006).

[26]E. Sonder, R. A. Zhur, and R. E. Valiga, "Annealing of damage and stability of implanted ions in ZnO crystals," J. Appl. Phys. **64**, 1140 (1988).

[27]A. Y. Azarov, S. O. Kucheyev, A. I. Titov, and P. A. Karaseov, "Effect of the density of collision cascades on ion implantation damage in ZnO," J. Appl. Phys. **102**, 083547 (2007).

[28]A. Y. Azarov, A. I. Titov, P. A. Karaseov, S. O. Kucheyev, A. Hallén, A. Y. Kuznetsov, B. G. Svensson, and A. P. Pathak, "Structural damage in ZnO bombarded by heavy ions," Vacuum **84**, 1058 (2010).

Published under license by AIP Publishing.

[29]A. Y. Azarov, P. T. Neuvonen, K. E. Knutsen, L. Vines, B. G. Svensson, and A. Y. Kuznetsov, "Impurity sublattice localization in ZnO revealed by Li marker diffusion," Phys. Rev. Lett. **110**, 175503 (2013).
[30]M. D. Giles, "Transient phosphorus diffusion below the amorphization threshold," J. Electrochem. Soc. **138**, 1160 (1991).
[31]P. T. Neuvonen, L. Vines, V. Venkatachalapathy, A. Zubiaga, F. Tuomisto, A. Hallén, B. G. Svensson, and A. Y. Kuznetsov, "Defect evolution and impurity migration in Na-implanted ZnO," Phys. Rev. B **84**, 205202 (2011).
[32]J. Kennedy, P. P. Murmu, E. Manikandan, and S. Y. Lee, "Investigation of structural and photoluminescence properties of gas and metal ions doped zinc oxide single crystals," J. Alloys Compd. **616**, 614 (2014).
[33]A. Y. Azarov, A. Hallén, Z. L. Liu, X. L. Du, B. G. Svensson, and A. Y. Kuznetsov, "Thermally induced surface instability in ion implanted $Mg_xZn_{1-x}O$ films," Phys. Rev. B **84**, 014114 (2011).
[34]J. Kennedy, D. A. Carder, A. Markwitz, and R. J. Reeves, "Properties of nitrogen implanted and electron beam annealed bulk ZnO," J. Appl. Phys. **107**, 103518 (2010).
[35]C. J. Pan, J. Y. Chen, G. C. Chi, B. W. Chou, B. J. Pong, F. Ren, C. Y. Chang, and S. J. Pearton, Vacuum **83**, 1073 (2009).
[36]K. Schmid, "Some new aspects for the evaluation of disorder profiles in silicon by backscattering," Radiat. Eff. **17**, 201 (1973).
[37]The correlation between lattice recovery and outdiffusion of Er atoms has been observed previously (Refs. 16 and 19), and this effect is out of scope of the present work.
[38]K. S. Chan, L. Vines, L. Li, C. Jagadish, B. G. Svensson, and J. Wong-Leung, "Zn precipitation and Li depletion in Zn implanted ZnO," Appl. Phys. Lett. **109**, 022102 (2016).
[39]P. T. Neuvonen, L. Vines, B. G. Svensson, and A. Y. Kuznetsov, "Intrinsic point-defect balance in self-ion-implanted ZnO," Phys. Rev. Lett. **110**, 015501 (2013).
[40]M. G. Wardle, J. P. Goss, and P. R. Briddon, "Theory of Li in ZnO: A limitation for Li-based *p*-type doping," Phys. Rev. B **71**, 155205 (2005).
[41]T. Moe Børseth, F. Tuomisto, J. S. Christensen, W. Skorupa, E. V. Monakhov, B. G. Svensson, and A. Y. Kuznetsov, "Deactivation of Li by vacancy clusters in ion-implanted and flash-annealed ZnO," Phys. Rev. B **74**, 161202(R) (2006).
[42]P. P. Michałowski, J. Gaca, M. Wójcik, and A. Turos, "Oxygen out-diffusion and compositional changes in zinc oxide during ytterbium ions bombardment," Nanotechnology **29**, 425710 (2018).
[43]L. A. Christel and J. F. Gibbons, "Stoichiometric disturbances in ion implanted compound semiconductors," J. Appl. Phys. **52**, 5050 (1981).
[44]A. Azarov, L. Vines, P. Rauwel, E. Monakhov, and B. G. Svensson, "Silver migration and trapping in ion implanted ZnO single crystals," J. Appl. Phys. **119**, 185705 (2016).
[45]V. Venkatachalapathy, A. Galeckas, M. Trunk, T. Zhang, A. Azarov, and A. Y. Kuznetsov, "Understanding phase separation in ZnCdO by a combination of structural and optical analysis," Phys. Rev. B **83**, 125315 (2011).
[46]J. F. Ziegler, J. P. Biersack, and U. Littmark, *The Stopping and Range of Ions in Solids* (Oxford, Pergamon, 1985), Vol. 1, p. 109, see www.srim.org.
[47]A. Azarov, E. Wendler, E. Monakhov, and B. G. Svensson, "Defect stabilization and reverse annealing in ZnO implanted with nitrogen at room and cryogenic temperature," J. Appl. Phys. **123**, 105701 (2018).
[48]D. B. Potter, M. J. Powell, J. A. Darr, I. P. Parkin, and C. J. Carmalt, "Transparent conducting oxide thin films of Si doped ZnO prepared by aerosol assisted CVD," RSC Adv. **7**, 10806 (2017).
[49]M. Jiang, D. D. Wang, Z. Q. Chen, S. Kimura, Y. Yamashita, A. Mori, and A. Uedono, "Chemical effect of Si^+ ions on the implantation-induced defects in ZnO studied by a slow positron beam," J. Appl. Phys. **113**, 043506 (2013).
[50]Y. Izawa, K. Matsumoto, K. Kuriyama, and K. Kushida, "Evaluation of zinc interstitial in Si-ion implanted ZnO bulk single crystals by a Rutherford backscattering study: An origin of low resistivity," Nucl. Instrum. Methods B **268**, 2104 (2010).
[51]A. Janotti and C. G. Van de Walle, "Native point defects in ZnO," Phys. Rev. B **76**, 165202 (2007).
[52]C. Bhoodoo, A. Hupfer, L. Vines, E. V. Monakhov, and B. G. Svensson, "Evolution kinetics of elementary point defects in ZnO implanted with low fluences of helium at cryogenic temperature," Phys. Rev. B **94**, 205204 (2016).

Published under license by AIP Publishing.